

1 Favorable Conditions for Magnetic Reconnection at Ganymede's Upstream Magnetopause

2

3 N. Kaweeyanun<sup>1</sup>, A. Masters<sup>1</sup>, X. Jia<sup>2</sup>

4

5 <sup>1</sup>Department of Physics, Imperial College London, Prince Consort Road, London, UK.

6 <sup>2</sup>Department of Climate and Space Sciences and Engineering, University of Michigan, Ann  
7 Arbor, Michigan, USA.

8

9 Corresponding author: N. Kaweeyanun

10 Corresponding author email: nk2814@ic.ac.uk

11

## 12 **Key Points**

- 13 • We create the first analytical model of conditions at Ganymede-Jupiter magnetopause  
14 and assess magnetic reconnection onset theory.
- 15 • Reconnection may occur anywhere on the magnetopause where Ganymede's closed  
16 magnetic field meets the ambient field of Jupiter.
- 17 • The average reconnection rate at Ganymede exhibits a Jovian-diurnal variation and  
18 hence is driven by Jupiter's rotation.

## 19 **Abstract**

20 Ganymede is the only Solar System moon known to generate a permanent magnetic field.  
21 Jovian plasma motions around Ganymede create an upstream magnetopause, where energy  
22 flows are thought to be driven by magnetic reconnection. Simulations indicate Ganymedean  
23 reconnection events may be transient, but the nature of magnetopause reconnection at  
24 Ganymede remains poorly understood, requiring an assessment of reconnection onset theory.  
25 We present an analytical model of steady-state conditions at Ganymede's magnetopause,  
26 from which the first Ganymedean reconnection onset assessment is conducted. We find that  
27 reconnection may occur wherever Ganymede's closed magnetic field encounters Jupiter's  
28 ambient magnetic field, regardless of variations in magnetopause conditions. Unrestricted  
29 reconnection onset highlights possibilities for multiple X-lines or widespread transient  
30 reconnection at Ganymede. The reconnection rate is controlled by the ambient Jovian field  
31 orientation and hence driven by Jupiter's rotation. Future progress on this topic is highly  
32 relevant for the JUPiter ICy moon Explorer (JUICE) mission.

33

## 34 **Plain Language Summary**

35 Ganymede is the largest moon of Jupiter and the only Solar System moon that produces its  
36 own magnetic field. Ganymede's magnetic field is surrounded by Jupiter's much larger  
37 magnetic field, which flows around the moon like a rock in a flowing river. The boundary  
38 where Jupiter's magnetic field first collides with Ganymede's is called the magnetopause. At  
39 this boundary, energy can move between the two magnetic fields through a process called  
40 magnetic reconnection. Our paper introduces a simple model of Ganymede's magnetopause,  
41 and use this to show where reconnection can occur on the boundary. We find that  
42 reconnection can occur anywhere on the magnetopause for any environmental conditions

43 around Ganymede, so the locations where these energy release events occur may be  
44 particularly unpredictable. The rate of energy release by reconnection meanwhile depends on  
45 near-Ganymede conditions, which change significantly as Jupiter rotates. These results will  
46 help inform the planning of the JUperiter ICy moon Explorer (JUICE) mission to Ganymede.

47

## 48 **Keywords**

49 Ganymede, magnetic reconnection, magnetopause, modeling

50

## 51 **1. Introduction**

52 Ganymede (radius  $R_G = 2,634$  km) is the largest moon of Jupiter (radius  $R_J = 71,492$  km) and  
53 the Solar System. Unlike all other moons, Ganymede generates a permanent magnetic field as  
54 discovered by measurements from both the magnetometer (Kivelson et al., 1997; Kivelson et  
55 al., 1996) and the plasma wave subsystem aboard the Galileo spacecraft (Gurnett et al.,  
56 1996). The permanent magnetic field is dipolar and likely produced by dynamo action within  
57 Ganymede's molten iron core (Anderson et al., 1996; Schubert et al., 1996). The equatorial  
58 surface dipole strength is 719 nT,  $\sim 7$  times stronger than the ambient Jovian magnetic field,  
59 and the dipole axis typically tilts  $\sim 176^\circ$  from Ganymede's spin axis (Kivelson et al., 2002).  
60 The dipole axis orientation varied over the short time scales between Galileo flybys, thought  
61 to be due to an additional, induced magnetic field arising from electromagnetic induction in a  
62 subsurface ocean (Kivelson et al., 2002). Obtaining detailed knowledge of this potentially  
63 life-sustaining water source is the primary objective for the upcoming JUperiter ICy moon  
64 Explorer (JUICE) mission, which will be the first spacecraft to orbit a non-Earth moon  
65 (Grasset et al., 2013).

66

67 Ganymede orbits Jupiter at an average distance of  $\sim 15 R_J$  in a plane nearly coplanar to  
68 Jupiter's spin equator (Bills, 2005; McKinnon, 1997). The orbital plane is  $\sim 7^\circ$  inclined with  
69 respect to the central plane of a  $\sim 3 R_J$  thick, rotating Jovian magnetospheric plasma sheet  
70 produced by Io's volcanic activities (Kivelson et al., 2004). Hence, Ganymede effectively  
71 moves up and down through the plasma sheet experiencing large variations in the ambient  
72 plasma and magnetic conditions. Under ideal magnetohydrodynamic (MHD) theory, the  
73 presence of rotating plasma sheet leads to outward stretching of Jovian magnetic field lines,  
74 forming a very strong ( $> 160$  MA) but thin current sheet approximately coplanar to the  
75 plasma sheet's central plane (Khurana et al., 2004). Hence, the ambient Jovian magnetized  
76 plasma conditions at Ganymede are controlled by the distance between Ganymede and the  
77 center of Jupiter's current sheet.

78

79 The Jovian plasma rotates with the planet at  $\sim 80\%$  of Jupiter's rotation speed (Williams,  
80 Mauk, McEntrie, 1997; Williams, Mauk, McEntrie, Roelof, et al., 1997), which is much  
81 faster than Ganymede's Keplerian speed. Hence, the magnetic field-carrying plasma  
82 compresses Ganymede's magnetic field on the upstream side forming a magnetopause  
83 boundary (Jia et al., 2008). The Jovian plasma is sub-Alfvénic so the magnetic pressure  
84 predominantly shapes magnetopause interactions (Neubauer, 1998). As a result, Ganymede's  
85 magnetosphere is cylindrically-shaped with long Alfvén wings and no bow shock preceding  
86 the magnetopause (Jia, Kivelson, et al., 2010) - a contrast to planetary magnetospheres which  
87 are bullet-shaped due to dynamic pressure dominance in the super-Alfvénic solar wind  
88 (Neubauer, 1990). Magnetic field lines near the upstream equator inside the magnetosphere  
89 are closed (both ends at Ganymede's magnetic poles) and almost antiparallel (due to  $176^\circ$

90 dipole tilt) to Jupiter's magnetic field lines. The nearly antiparallel configuration hints that  
91 magnetic reconnection may be the dominant mechanism for plasma and energy inflows from  
92 Jupiter to Ganymede. Elsewhere, magnetic field lines in Ganymede's large polar caps and  
93 magnetotail are open (at least one end at Jupiter), allowing particles to enter and escape from  
94 the moon's magnetosphere (Frank et al., 1997; Williams, Mauk, McEntrie, 1997; Williams,  
95 Mauk, McEntrie, Roelof, et al., 1997).

96

97 The Ganymede magnetosphere has been modeled by many numerical simulations, some of  
98 which discuss magnetic reconnection at the upstream magnetopause. For instance, Jia et al.  
99 (2008; 2009) produced a global three-dimensional resistive MHD simulation of Ganymede  
100 that showed transient reconnection signatures spread over large regions of the magnetopause.  
101 Subsequent analysis revealed these signals to be consistent with intermittent rope-like flux-  
102 transfer events (Jia, Walker, et al., 2010). Recently, modeling work has been extended to  
103 include the Hall effect (Dorelli et al., 2015), and to couple with kinetic-ion hybrid (Leclercq  
104 et al., 2016) and local particle-in-cell codes (Daldorff et al., 2014; Tóth et al., 2016; Zhou et  
105 al., 2019), all of which treat reconnection microphysics more directly. The Hall-MHD model  
106 predicted local ion accelerations from reconnection, while the MHD-EPIC (embedded  
107 particle-in-cell) model suggested particle heating from reconnection and presence of  
108 quasiperiodic formation of flux-transfer events consistent with previous resistive MHD  
109 results and Galileo observations. However, these comprehensive numerical modelling studies  
110 have not been supported by important assessment of reconnection at Ganymede's  
111 magnetopause that apply reconnection onset theory, which is an essential additional element  
112 in understanding the physics at work.

113

114 We have used an analytical approach to parametrize the magnetopause conditions expected  
 115 from a typical Jovian plasma flow. This approach provides a computationally cheap way to  
 116 apply modern kinetic physics of reconnection onset that is challenging to implement in more  
 117 expensive numerical models. Reconnection onset has been analytically assessed at Earth  
 118 (Alexeev et al., 1998; Trattner et al., 2007a, 2007b), Jupiter (Desroche et al., 2012; Masters,  
 119 2017), Saturn (Desroche et al., 2013; Masters, 2015a), Uranus (Masters, 2014), and Neptune  
 120 (Masters, 2015b). In the following sections, we outline the analytical model of Ganymede’s  
 121 upstream magnetopause followed by the first kinetic assessment of magnetic reconnection  
 122 onset and structural properties.

123

## 124 **2. Analytical Model of Ganymede’s Upstream Magnetopause**

125 Maps of conditions immediately either side of Ganymede’s magnetopause are essential for  
 126 reconnection onset assessment. To achieve this, we must first define the magnetopause  
 127 surface itself. Kivelson et al. (1998) describe Ganymede’s magnetosphere as a cylinder with  
 128 shifting center points in a dynamical Ganymede-centered Jovian magnetic field-aligned  
 129 coordinates (GphiB). This is converted to a Ganymede-centered Cartesian coordinates  
 130 (GphiO) for our model in which X points along the plasma flow direction, Y points from  
 131 Ganymede to Jupiter, and Z points along Jupiter’s spin axis (approximately parallel to  
 132 Ganymede’s spin axis due to the moon’s small orbit inclination). The shape of Ganymede’s  
 133 magnetopause surface follows

$$f(X, Y, Z) = \frac{(X - X_0)^2}{a^2} + \frac{(Y \cos \theta_r - Z \sin \theta_r - Y_0)^2}{b^2} = 1$$

134 where

$$\theta_r = \tan^{-1} \left( \frac{|B_{0,z}|}{B_{0,y}} \right) - 90^\circ$$

$$X_0(Y, Z) = X_0(0) + |Y \sin \theta_r + Z \cos \theta_r| \tan \theta$$

$$Y_0(Y, Z) = \frac{2}{\pi} Y_{0,max} \sin(\phi - 248^\circ) \tan^{-1} \left( \frac{Y \sin \theta_r + Z \cos \theta_r}{\lambda} \right)$$

135 The angle  $\theta_r$  describes right-handed rotation angle between GphiB and GphiO coordinates  
 136 where  $(B_{0,y}, B_{0,z})$  are the ambient Jovian magnetic field components.  $(X_0, Y_0)$  denote the  
 137 center point offsets from the GphiO origin. Kivelson et al. (1998) chose  $a = 2.2 R_G$  and  
 138  $\lambda = 0.5 R_G$ , and then used least square fit to the Galileo data to calculate  $b = 2.90 R_G$ ,  
 139  $X_0(0) = 0.544 R_G$ ,  $Y_{0,max} = 0.914 R_G$ , and  $\theta = 0.298$  radians. This leaves Jupiter's east  
 140 longitude  $\phi$ , which captures north-south asymmetry of Ganymede's magnetosphere in  
 141 response to the ambient Jovian magnetic field orientation, as the only free parameter. Each  $\phi$   
 142 value importantly corresponds to a unique position of Ganymede with respect to the Jovian  
 143 current sheet.

144

145 From these equations we can generate Ganymede's upstream ( $X < 0 R_G$ ) magnetopause grid  
 146 surface between  $-4.0 R_G < Y < 4.0 R_G$  and  $-1.0 R_G < Z < 1.0 R_G$  with  $0.01 R_G$  resolution  
 147 in both dimensions. The magnetopause is projected onto a Y-Z plane as shown in Figure 1A  
 148 specifically when Ganymede is in the Jovian current sheet ( $\phi = 248^\circ$ ). Here the  
 149 magnetopause is north-south symmetric with the standoff distance of  $1.65 R_G$  calculated at  
 150 the subflow point ( $Y = 0 R_G, Z = 0 R_G$ ). The magnetopause X-coordinate increases away  
 151 from the subflow point in all directions as the surface curves downstream. The magnetopause  
 152 will gain maximum north-south asymmetries when Ganymede is furthest above/below the  
 153 current sheet ( $\phi = 158^\circ, 338^\circ$ ). This simple and fixed magnetopause description is sufficient

154 for reconnection onset assessment, as more accurate surface models will not affect the  
155 conclusions drawn.

156

157 Next, we describe the Jovian-side (external) conditions at the magnetopause. The ambient  
158 Jovian plasma mass density is  $\rho_0 = 56 \text{ amu/cm}^3$  when Ganymede is in the current sheet and  
159  $\rho_0 = 28 \text{ amu/cm}^3$  when Ganymede is furthest above/below the current sheet (Jia et al., 2008).  
160 The plasma is compressed near Ganymede's magnetopause increasing its mass density. We  
161 employ a simple compression formula  $\rho_J = A_1 \cos(\alpha) + \rho_0$  where  $\alpha$  is the flaring angle  
162 between the X-axis and the local magnetopause normal vector. The cosine of flaring angle is  
163 adapted from results at Earth's magnetopause (Petrinec & Russell, 1997) and captures spatial  
164 density variations expected from plasma flows around a cylindrical magnetosphere. A more  
165 complex compression description is again possible but unlikely to affect main conclusions  
166 drawn. The typical compression amplitude  $A_1 = 4 \text{ amu/cm}^3$  is estimated from numerical  
167 simulations (Jia et al., 2008; Tóth et al., 2016) and the added ambient mass density  $\rho_0$  forbid  
168 plasma decompression. Figure 1B shows the Jovian-side mass density variation when  
169 Ganymede is in the current sheet. The density peaks near the subflow point where Jovian  
170 plasma collides head-on with the magnetopause and decreases toward the flanks where  
171 plasma glances off the surface.

172

173 The ambient Jovian plasma pressure is  $P_0 = 3.8 \text{ nPa}$  when Ganymede is in the current sheet  
174 and  $P_0 = 1.9 \text{ nPa}$  when Ganymede is furthest above/below the current sheet (Jia et al., 2008;  
175 Kivelson et al., 2004). Figure 1C shows plasma pressure at the Jovian-side magnetopause  
176 when Ganymede is in the current sheet. Like mass density, a cosine relation  $P_{J,p} =$   
177  $A_2 \cos(\alpha) + P_0$  parametrizes the pressure compression. The amplitude  $A_2 = 1.0528 \text{ nPa}$  is

178 approximated from the pressure relation at Earth's magnetopause for slow plasma flow  
179 speeds (Petrinec & Russell, 1997).

180

181 The ambient Jovian plasma flows along the X-axis at speed  $v_0 = 140$  km/s in Ganymede's  
182 reference frame (Jia et al., 2008). Figure 1D shows the plasma flow velocity at the Jovian-  
183 side magnetopause when Ganymede is in the current sheet. Unlike mass density and pressure,  
184 we parametrize the flow speed by a sine relation  $v_J = v_0 \sin(\alpha)$  as the ambient plasma is most  
185 stagnated by direct collision near the subflow point. The Jovian-side flow directions (denoted  
186 by arrows normalized in the Y-Z plane) are constrained parallel to the magnetopause surface  
187 and coplanar to the ambient plasma flow vector.

188

189 The ambient Jovian magnetic field has been computed at Ganymede using a mathematical  
190 model (Jia et al., 2008; Khurana, 1997). The magnetic field strength is a function of Jupiter's  
191 east longitude and hence Ganymede's orbital position, with minimum of  $B_0 \sim 70$  nT when  
192 Ganymede is in the current sheet and maximum of  $B_0 \sim 105$  nT when Ganymede is furthest  
193 above/below the current sheet. We assume negligible x-component  $B_{0,x}$  and parametrize the  
194 remaining two components by  $B_{0,y} = 84 \sin(\phi - 248^\circ)$  nT and  $B_{0,z} = 3 \cos(\phi) - 79$  nT.  
195 Since  $B_{0,z}$  is always negative, the ambient Jovian magnetic field points southward in the Y-Z  
196 plane between  $135^\circ$ - $225^\circ$  clock angles. We quantify magnetic field compression at the  
197 Jovian-side magnetopause using the fact that the sum of magnetic, plasma, and dynamic  
198 pressures must be equal before and after the compression. The total pre-compression pressure  
199 can be calculated from ambient plasma/magnetic values. Using data from Figures 1C and 1D,  
200 we derive post-compression plasma pressure and magnetopause-parallel dynamic pressure  
201 component. We subtract these values from the total pressure to obtain the post-compression

202 magnetic pressure  $P_{J,b}$  (which also contains the magnetopause-normal dynamic pressure  
203 component) and convert this into Jovian-side magnetic field strength  $B_J$  shown in Figure 1E  
204 when Ganymede is in the current sheet. The plasma compression also constrains magnetic  
205 field directions onto the magnetopause surface, which we denote by normalized arrows.

206

207 The Jovian-side plasma and magnetic pressures together exert force on Ganymede's  
208 magnetopause, which is balanced by magnetic pressure from Ganymede's magnetic field  
209 given negligible plasma pressure inside the moon's magnetosphere (Jia et al., 2008). Hence,  
210 we can derive the magnetic field strength at the Ganymede-side magnetopause  $B_G$  as  
211 shown in Figure 1F when Ganymede is in the current sheet. Magnetic field directions  
212 (normalized arrows) have no azimuthal component (consistent with dipolar field) and lie  
213 parallel to the magnetopause surface. The magnetic field points northward in the "closed-  
214 field region" defined by  $|Z| < 0.63 R_G$  and southward elsewhere. The closed-field region is  
215 bounded by two horizontal red dashed lines which we retroactively add to all Figure 1  
216 subplots. Otherwise, the Ganymede-side plasma density and flow speed are set to uniform  
217 values  $\rho_G = 20 \text{ amu/cm}^3$  and  $v_G = 0 \text{ km/s}$  respectively - the latter approximates a relatively  
218 slow plasma flow inside Ganymede's magnetosphere compared to the external Jovian flow.

219

### 220 **3. Magnetic Reconnection Assessment at Ganymede**

221 Having obtained maps of conditions on both sides of Ganymede's magnetopause, we can  
222 assess reconnection onset specifically for the closed-field region where particle transport is  
223 not expected under MHD theory. Reconnection onset requires three conditions to be satisfied.  
224 First, the magnetopause current sheet separating Jupiter's and Ganymede's magnetic fields  
225 must be thinner than approximately an ion inertial length to break the MHD frozen-in flux

226 condition and allow collisionless plasma diffusion (Phan et al., 2011). The Galileo data  
 227 analysis revealed the magnetopause current sheet thickness to be <400 km (Kivelson et al.,  
 228 1998), similar to the ~426 km ion inertial length calculated from magnetopause conditions in  
 229 Figure 1. Hence, we can assume a sufficiently thin magnetopause current sheet irrespective of  
 230 Ganymede's position relative to the Jovian current sheet.

231

232 The remaining two onset conditions effectively limit local plasma flows to below the  
 233 characteristic Alfvén speed associated with reconnection, with suppression of reconnection  
 234 above this limit. The second onset condition concerns the diamagnetic drift between plasma  
 235 electrons and ions within the magnetopause current sheet, leading to a condition involving the  
 236 magnetic shear angle

$$\theta_{\text{sh}} > 2 \tan^{-1} \left( \frac{d_i \Delta\beta}{L} \right) = 2 \tan^{-1}(\Delta\beta)$$

237 where  $\theta_{\text{sh}}$  is the smaller shear angle between the Jovian and Ganymedean magnetic fields in a  
 238 magnetopause-tangent plane at each grid point (Swisdak et al., 2003; 2010). If this condition  
 239 is unsatisfied, the diamagnetic drift is too fast and reconnection is suppressed. The system  
 240 length scale ( $L$ ) is the magnetopause current sheet thickness, which from the first onset  
 241 condition is approximately equal to the ion inertial length ( $d_i$ ), so the shear angle minimum  
 242 threshold depends only on the beta difference ( $\Delta\beta = \beta_J - \beta_G$ ) across the magnetopause. As  
 243 Ganymede contributes negligible plasma pressure ( $\beta_G = 0$ ), the beta difference is equal to the  
 244 Jovian-side beta  $\beta_J = P_{J,p}/P_{J,b}$ . The third onset condition concerns the flow shear between  
 245 Jovian and Ganymedean bulk plasmas adjacent to the magnetopause current sheet along  
 246 reconnection outflow direction. Each magnetopause location has two outflow vectors  
 247 parallel/antiparallel to the cross product of the vector bisecting the smaller shear angle

248 between Jovian and Ganymedean magnetic field lines and the local surface normal vector  
 249 (Masters, 2017). We choose the southward-pointing primary outflow vector following the  
 250 Jovian field lines, and define the flow shear condition

$$v_{\text{sh}} = \frac{|v_1 - v_2|}{2} < v_{\text{out}} \left( \frac{\rho_1 B_2 + \rho_2 B_1}{2(\rho_1 B_2 \rho_2 B_1)^{1/2}} \right)$$

$$v_{\text{out}} = \left( \frac{B_1 B_2 (B_1 + B_2)}{\mu_0 (\rho_1 B_2 + \rho_2 B_1)} \right)^{1/2}$$

251 where symbol definitions are  $v$  = flow velocity,  $\rho$  = mass density,  $B$  = magnetic field  
 252 strength, and  $\mu_0 = 4\pi \times 10^{-7}$  H/m (Doss et al., 2015). Subscripts 1 and 2 indicate parameter  
 253 projections along the outflow vector on Jovian-side and Ganymedean-side respectively. The  
 254 flow shear is  $v_{\text{sh}} = |v_1 - v_2|/2$  and the outflow speed is  $v_{\text{out}}$ . Reconnection is suppressed if  
 255 the flow shear exceeds its maximum threshold.

256

257 We first assess these two onset conditions for a specific case when Ganymede is in the Jovian  
 258 current sheet, and then consider two extreme cases when Ganymede is furthest above/below  
 259 the current sheet. Figure 2 assesses the diamagnetic drift condition when Ganymede is in the  
 260 current sheet. Beta differences in Figure 2A have the average of 2.02 in the closed-field  
 261 region, with largest discrepancies along the magnetopause flanks where the Jovian-side  
 262 magnetic field is weakest. The resulting shear angle minimum thresholds ( $\theta_{\text{sh,min}}$ ) in Figure  
 263 2B have the average of  $90.3^\circ$  with largest values along the flanks. Figure 2C shows magnetic  
 264 shear angles calculated using data from Figures 1E and 1F. The average  $\theta_{\text{sh}}$  is  $175^\circ$  with  
 265 largest values in columns nearest to the subflow point and toward the flanks, with smaller  
 266 values in-between. Comparing Figures 2B and 2C indicates that  $\theta_{\text{sh}} > \theta_{\text{sh,min}}$  at every point

267 in the closed-field region, so the second onset condition is satisfied everywhere on  
 268 Ganymede's magnetopause.

269

270 Figure 3 assesses the flow shear condition when Ganymede is in the current sheet.  
 271 Reconnection outflow speeds in Figure 3A have the average of 327 km/s in the closed-field  
 272 region with largest values along columns near the subflow point, where magnetic fields are  
 273 most strongly aligned with outflow vectors. The resulting maximum flow shear thresholds  
 274 ( $v_{sh,max}$ ) in Figure 3B have the average of 443 km/s with largest values near the subflow  
 275 point. Figure 3C shows flow shears calculated from the Jovian plasma flow in Figure 1D. The  
 276 average  $v_{sh}$  is 13.7 km/s with largest values near the subflow point from outflow-aligned  
 277 magnetic fields. A zero-shear strip is present along  $Z = 0$  where the Jovian plasma flow  
 278 stagnates. Comparing Figures 3B and 3C indicates that  $v_{sh} < v_{sh,max}$  at every point in the  
 279 closed-field region, so the third onset condition is satisfied everywhere on Ganymede's  
 280 magnetopause.

281

282 Consequentially, magnetic reconnection can occur anywhere on Ganymede's magnetopause  
 283 when Ganymede is in the current sheet. The electric field associated with reconnection  
 284 follows (Doss et al., 2015)

$$E = 2k \left( \frac{B_1 B_2}{B_1 + B_2} \right) v_{out} \left( 1 - \frac{(v_1 - v_2)^2}{(v_{out})^2} \frac{\rho_1 B_2 \rho_2 B_1}{(\rho_1 B_2 + \rho_2 B_1)^2} \right)$$

285 Where  $k = 0.1$  is the reconnection efficiency factor (Paschmann et al., 2013). Figure 4A  
 286 shows the electric field when Ganymede is in the current sheet with average magnitude 3.2  
 287 mV/m. Strongest field magnitudes are found along near-subflow columns corresponding to

288 largest outflow speed locations. We also track (following Cooling et al., 2001) parcels of  
289 plasma in reconnection outflows from three equatorial reconnection sites – one at the subflow  
290 point and two others at mid-flanks ( $Y = \pm 1.5 R_G$ ). All outflows travel bidirectionally  
291 north/south away from Ganymede's equator. However, the subflow site's outflows remain on  
292 the magnetopause symmetry axis ( $Z = 0$ ) while the mid-flank sites' outflows shift toward  
293 their nearest flanks due to influence from the Jovian-side plasma flow.

294

295 Figures 4B and 4C respectively show reconnection assessment when Ganymede is furthest  
296 above and below the current sheet, with magnetopause asymmetries and ambient parameters  
297 adjusted accordingly. Despite condition changes, the electric fields remain non-zero  
298 throughout closed-field regions, so reconnection is possible anywhere on the magnetopause  
299 when Ganymede is furthest above/below the current sheet. The electric field varies  
300 symmetrically north/south of the current sheet and becomes stronger along the flanks where  
301 Jupiter's and Ganymede's magnetic fields are now most strongly antiparallel. The average  
302 electric field also increases from 3.2 mV/m to 5.1 mV/m at extreme Ganymede positions.  
303 Small discontinuities are observed across lines containing the subflow point, reflecting sharp  
304 turns on the magnetopause arising from the surface equations. A more realistic magnetopause  
305 surface would be smoother, and so the discontinuities should disappear.

306

#### 307 **4. Discussion**

308 There appears to be no restrictions for reconnection onset when Ganymede's magnetosphere  
309 is symmetric (Figure 4A) and most asymmetric (Figures 4B and 4C). Hence, we can  
310 generalize that reconnection is favorable anywhere on the magnetopause for all  
311 magnetospheric asymmetries i.e. all positions along Ganymede's orbit of Jupiter. This result

312 is consistent with widespread reconnection events observed in global simulations (e.g. Jia,  
313 Walker, et al., 2010; Tóth et al., 2016)

314

315 The electric field magnitude range (2.6 – 5.6 mV/m) observed are much larger compared to at  
316 Earth's (<0.01 – 0.2 mV/m) and Jupiter's (<0.1 mV/m) upstream magnetopauses (Paschmann  
317 et al., 2013; Masters, 2017), indicating significant reconnection rates at all Ganymede  
318 magnetopause locations. Although a dominant X-line is possible, this electric field  
319 configuration highlights possibilities for less ordered reconnection site distributions, such as  
320 multiple X-lines or transient flux-transfer events (seen in global simulations), at Ganymede's  
321 magnetopause.

322

323 The electric field equation is found most sensitive to changes in magnetic parameters  $B_1$  and  
324  $B_2$ . Due to the model's fixed magnetopause surface, both  $B_1$  and  $B_2$  increase with stronger  
325 ambient Jovian magnetic field as Ganymede moves away from the Jovian current sheet. The  
326 average electric field increases in Figure 4 are therefore monotonic and functions of  
327 Ganymede's orbital position and Jupiter's east longitude similar to the ambient Jovian  
328 magnetic field strength. As each longitude value also corresponds to distinct time-of-day on  
329 Jupiter, magnetic reconnection rate at Ganymede exhibits a Jovian-diurnal variation and is  
330 effectively driven by Jupiter's rotation. The conclusion has been independently supported by  
331 remote observations of Jovian radio emissions associated with Ganymede (Zarka et al.,  
332 2018).

333

334 Multiplying the average electric fields by the magnetopause width ( $\sim 6 R_G$ ) gives 50-80 kV  
335 reconnection voltage estimates at Ganymede's magnetopause, which may be used to

336 constrain reconnection rate in the magnetotail via open magnetic flux conservation. We also  
337 calculate reconnection-induced electron and ion temperature increases of 250-560 eV and  
338 2,000-4,200 eV respectively using empirical methods from Earth-based studies (Phan et al.,  
339 2013; 2014), with the maximum (minimum) value corresponds to when Ganymede is furthest  
340 above/below (in) the Jovian current sheet. These numbers far exceed ambient temperatures  
341 for electrons and ions of 300 eV and 60 eV respectively (Kivelson et al., 2004), hence  
342 reconnection should provide heated particle signatures observable by the upcoming JUICE  
343 mission.

344

## 345 **5. Summary**

346 Ganymede's permanent magnetic field and its resulting magnetosphere present a unique  
347 opportunity to study magnetic reconnection in a sub-Alfvénic plasma flow environment. We  
348 present an analytical model of steady-state conditions at Ganymede's upstream  
349 magnetopause, from which we conduct the first assessment of reconnection onset theory at  
350 this boundary. The model shows that reconnection may occur anywhere on the magnetopause  
351 where Ganymede's closed magnetic field encounters Jupiter's ambient field, and the onset  
352 appears largely unaffected by Ganymede's position relative to the Jovian current sheet. This  
353 result is consistent with previous global MHD simulations of Ganymede's magnetosphere,  
354 and highlights possibilities for less orderly reconnection structures (multiple X-lines,  
355 widespread flux-transfer events) at Ganymede's magnetopause.

356

357 The average reconnection rate is shown to be a function of Ganymede's position along its  
358 orbit around Jupiter, which approximately corresponds to the time-of-day on Jupiter. Hence,  
359 the reconnection rate exhibits a Jovian-diurnal variation and is effectively driven by Jupiter's

360 rotation. The reconnection process should heat up surrounding plasma particles producing  
361 signatures detectable by spacecraft instruments. Our steady-state model currently does not  
362 capture orientation changes of Ganymede's magnetic field due to the moon's subsurface  
363 ocean. Future integration of ocean effects will allow more accurate predictions of  
364 reconnection structures in preparation for the JUICE space mission.

365

### 366 **Acknowledgements**

367 NK is supported by a Royal Society PhD Studentship, and AM is supported by a Royal  
368 Society University Research Fellowship. Derived data shown in Figures 1-4 is available in  
369 the supporting information.

370 **Reference**

- 371 Alexeev, I. I., Sibeck, D. G., & Bobrovnikov, S. Y. (1998). Concerning the location of  
372 magnetopause merging as a function of the magnetopause current strength. *Journal of*  
373 *Geophysical Research: Space Physics*, *103*(A4), 6675--6684. doi:10.1029/97JA02863
- 374 Anderson, J. D., Lau, E. L., Sjogren, W. L., Schubert, G., & Moore, W. B. (1996).  
375 Gravitational constraints on the internal structure of Ganymede. *Nature*, *384*(6609),  
376 541--543. doi:10.1038/384541a0
- 377 Bills, B. G. (2005). Free and forced obliquities of the Galilean satellites of Jupiter. *Icarus*,  
378 *175*(1), 233--247. doi:10.1016/j.icarus.2004.10.028
- 379 Cooling, B. M. A., Owen, C. J., & Schwartz, S. J. (2001). Role of the magnetosheath flow in  
380 determining the motion of open flux tubes. *Journal of Geophysical Research: Space*  
381 *Physics*, *106*(A9), 18763--18775. doi:10.1029/2000JA000455
- 382 Daldorff, L. K. S., Tóth, G., Gombosi, T. I., Lapenta, G., Amaya, J., Markidis, S., &  
383 Brackbill, J. U. (2014). Two-way coupling of a global Hall magnetohydrodynamics  
384 model with a local implicit particle-in-cell model. *Journal of Computational Physics*,  
385 *268*, 236--254. doi:10.1016/j.jcp.2014.03.009
- 386 Desroche, M., Bagenal, F., Delamere, P. A., & Erkaev, N. (2012). Conditions at the expanded  
387 Jovian magnetopause and implications for the solar wind interaction. *Journal of*  
388 *Geophysical Research: Space Physics*, *117*(A7). doi:10.1029/2012JA017621
- 389 Desroche, M., Bagenal, F., Delamere, P. A., & Erkaev, N. (2013). Conditions at the  
390 magnetopause of Saturn and implications for the solar wind interaction. *Journal of*  
391 *Geophysical Research: Space Physics*, *118*(6), 3087--3095. doi:10.1002/jgra.50294
- 392 Dorelli, J. C., Glocer, A., Collinson, G., & Tóth, G. (2015). The role of the Hall effect in the  
393 global structure and dynamics of planetary magnetospheres: Ganymede as a case

394 study: Hall reconnection at Ganymede. *Journal of Geophysical Research: Space*  
395 *Physics*, 120. doi:10.1002/2014JA020951

396 Doss, C. E., Komar, C. M., Cassak, P. A., Wilder, F. D., Eriksson, S., & Drake, J. F. (2015).  
397 Asymmetric magnetic reconnection with a flow shear and applications to the  
398 magnetopause. *Journal of Geophysical Research: Space Physics*, 120(9), 7748--7763.  
399 doi:10.1002/2015JA021489

400 Frank, L. A., Paterson, W. R., Ackerson, K. L., & Bolton, S. J. (1997). Outflow of hydrogen  
401 ions from Ganymede. *Geophysical Research Letters*, 24(17), 2151--2154.  
402 doi:10.1029/97GL01744

403 Grasset, O., Dougherty, M. K., Coustenis, A., Bunce, E., Erd, C., Titov, D. V., . . . Van  
404 Hoolst, T. (2013). JUPITER ICY moons Explorer (JUICE): An ESA mission to orbit  
405 Ganymede and to characterise the Jupiter system. *Planetary and Space Science*, 78, 1-  
406 -21. doi:10.1016/j.pss.2012.12.002

407 Gurnett, D. A., Kurth, W. S., Roux, A., Bolton, S. J., & Kennel, C. F. (1996). Evidence for a  
408 magnetosphere at Ganymede from plasma-wave observations by the Galileo  
409 spacecraft. *Nature*, 384(6609), 535--537. doi:10.1038/384535a0

410 Jia, X., Kivelson, M. G., Khurana, K. K., & Walker, R. J. (2010). Magnetic Fields of the  
411 Satellites of Jupiter and Saturn. *Space Science Reviews*, 152(1), 271--305.  
412 doi:10.1007/s11214-009-9507-8

413 Jia, X., Walker, R. J., Kivelson, M. G., Khurana, K. K., & Linker, J. A. (2008). Three-  
414 dimensional MHD simulations of Ganymede's magnetosphere. *Journal of*  
415 *Geophysical Research: Space Physics*, 113(A6). doi:10.1029/2007JA012748

416 Jia, X., Walker, R. J., Kivelson, M. G., Khurana, K. K., & Linker, J. A. (2009). Properties of  
417 Ganymede's magnetosphere inferred from improved three-dimensional MHD

418 simulations. *Journal of Geophysical Research: Space Physics*, 114(A9).  
419 doi:10.1029/2009JA014375

420 Jia, X., Walker, R. J., Kivelson, M. G., Khurana, K. K., & Linker, J. A. (2010). Dynamics of  
421 Ganymede's magnetopause: Intermittent reconnection under steady external  
422 conditions. *Journal of Geophysical Research: Space Physics*, 115(A12).  
423 doi:10.1029/2010JA015771

424 Khurana, K., M. Vasyliūnas, V., H. Mauk, B., Frank, L., Paterson, B., G. Kivelson, M., . . .  
425 Kurth, B. (2004). The configuration of Jupiter's magnetosphere. *Jupiter: The Planet,*  
426 *Satellites and Magnetosphere*, 593-616 (2004).

427 Khurana, K. K. (1997). Euler potential models of Jupiter's magnetospheric field. *Journal of*  
428 *Geophysical Research: Space Physics*, 102(A6), 11295--11306.  
429 doi:10.1029/97JA00563

430 Kivelson, M. G., Bagenal, F., Kurth, W., M. Neubauer, F., Paranicas, C., & Saur, J. (2004).  
431 Magnetospheric interactions with satellites. *Jupiter. The Planet, Satellites and*  
432 *Magnetosphere*, 513-536.

433 Kivelson, M. G., Khurana, K. K., Coroniti, F. V., Joy, S., Russell, C. T., Walker, R. J., . . .  
434 Polanskey, C. (1997). The magnetic field and magnetosphere of Ganymede.  
435 *Geophysical Research Letters*, 24(17), 2155--2158. doi:10.1029/97GL02201

436 Kivelson, M. G., Khurana, K. K., Russell, C. T., Walker, R. J., Warnecke, J., Coroniti, F. V.,  
437 . . . Schubert, G. (1996). Discovery of Ganymede's magnetic field by the Galileo  
438 spacecraft. *Nature*, 384(6609), 537--541. doi:10.1038/384537a0

439 Kivelson, M. G., Khurana, K. K., & Volwerk, M. (2002). The Permanent and Inductive  
440 Magnetic Moments of Ganymede. *Icarus*, 157(2), 507--522.  
441 doi:https://doi.org/10.1006/icar.2002.6834

442 Kivelson, M. G., Warnecke, J., Bennett, L., Joy, S., Khurana, K. K., Linker, J. A., . . .  
443 Polanskey, C. (1998). Ganymede's magnetosphere: Magnetometer overview. *Journal*  
444 *of Geophysical Research: Planets*, 103(E9), 19963--19972. doi:10.1029/98JE00227

445 Leclercq, L., Modolo, R., Leblanc, F., Hess, S., & Mancini, M. (2016). 3D magnetospheric  
446 parallel hybrid multi-grid method applied to planet-plasma interactions. *Journal of*  
447 *Computational Physics*, 309, 295-313. doi:https://doi.org/10.1016/j.jcp.2016.01.005

448 Masters, A. (2014). Magnetic reconnection at Uranus' magnetopause. *Journal of Geophysical*  
449 *Research: Space Physics*, 119(7), 5520--5538. doi:10.1002/2014JA020077

450 Masters, A. (2015a). The dayside reconnection voltage applied to Saturn's magnetosphere.  
451 *Geophysical Research Letters*, 42(8), 2577--2585. doi:10.1002/2015GL063361

452 Masters, A. (2015b). Magnetic reconnection at Neptune's magnetopause. *Journal of*  
453 *Geophysical Research: Space Physics*, 120(1), 479--493. doi:10.1002/2014JA020744

454 Masters, A. (2017). Model-Based Assessments of Magnetic Reconnection and Kelvin-  
455 Helmholtz Instability at Jupiter's Magnetopause. *Journal of Geophysical Research:*  
456 *Space Physics*, 122(11), 11,154--111,174. doi:10.1002/2017JA024736

457 McKinnon, W. B. (1997). Galileo at Jupiter ---meetings with remarkable moons. *Nature*,  
458 390(6655), 23--26. doi:10.1038/36222

459 Neubauer, F. (1998). *The sub-Alfvenic interaction of the Galilean satellites with the Jovian*  
460 *magnetosphere* (Vol. 103).

461 Neubauer, F. M. (1990). Satellite plasma interactions. *Advances in Space Research*, 10, 25--  
462 38. doi:10.1016/0273-1177(90)90083-C

463 Paschmann, G., Øieroset, M., & Phan, T. (2013). In-Situ Observations of Reconnection in  
464 Space. *Space Science Reviews*, 178(2), 385--417. doi:10.1007/s11214-012-9957-2

465 Petrinec, S. M., & Russell, C. T. (1997). Hydrodynamic and MHD equations across the bow  
466 shock and along the surface of planetary obstacles. *Space Science Reviews*, 79(3),  
467 757--791. doi:10.1023/A:1004938724300

468 Phan, T. D., Drake, J. F., Shay, M. A., Gosling, J. T., Paschmann, G., Eastwood, J. P., . . .  
469 Angelopoulos, V. (2014). Ion bulk heating in magnetic reconnection exhausts at  
470 Earth's magnetopause: Dependence on the inflow Alfvén speed and magnetic shear  
471 angle. *Geophysical Research Letters*, 41(20), 7002--7010.  
472 doi:10.1002/2014GL061547

473 Phan, T. D., Love, T. E., Gosling, J. T., Paschmann, G., Eastwood, J. P., Oieroset, M., . . .  
474 Auster, U. (2011). Triggering of magnetic reconnection in a magnetosheath current  
475 sheet due to compression against the magnetopause. *Geophysical Research Letters*,  
476 38(17). doi:10.1029/2011GL048586

477 Phan, T. D., Shay, M. A., Gosling, J. T., Fujimoto, M., Drake, J. F., Paschmann, G., . . .  
478 Angelopoulos, V. (2013). Electron bulk heating in magnetic reconnection at Earth's  
479 magnetopause: Dependence on the inflow Alfvén speed and magnetic shear.  
480 *Geophysical Research Letters*, 40(17), 4475--4480. doi:10.1002/grl.50917

481 Schubert, G., Zhang, K., Kivelson, M. G., & Anderson, J. D. (1996). The magnetic field and  
482 internal structure of Ganymede. *Nature*, 384(6609), 544--545. doi:10.1038/384544a0

483 Swisdak, M., Opher, M., Drake, J. F., & Alouani Bibi, F. (2010). The vector direction of the  
484 Interstellar Magnetic Field Outside the Heliosphere. *710(2)*, 1769-1775.  
485 doi:10.1088/0004-637x/710/2/1769

486 Swisdak, M., Rogers, B., F. Drake, J., & Shay, M. (2003). Diamagnetic Suppression of  
487 Component Magnetic Reconnection at the Magnetopause. *J. Geophys. Res.*, 108.  
488 doi:10.1029/2002JA009726

489 Tóth, G., Jia, X., Markidis, S., Peng, I. B., Chen, Y., Daldorff, L. K. S., . . . Dorelli, J. C.  
490 (2016). Extended magnetohydrodynamics with embedded particle-in-cell simulation  
491 of Ganymede's magnetosphere. *Journal of Geophysical Research: Space Physics*,  
492 *121*(2), 1273--1293. doi:10.1002/2015JA021997

493 Trattner, K. J., Mulcock, J. S., Petrinec, S. M., & Fuselier, S. A. (2007a). Location of the  
494 reconnection line at the magnetopause during southward IMF conditions. *Geophysical*  
495 *Research Letters*, *34*(3). doi:10.1029/2006GL028397

496 Trattner, K. J., Mulcock, J. S., Petrinec, S. M., & Fuselier, S. A. (2007b). Probing the  
497 boundary between antiparallel and component reconnection during southward  
498 interplanetary magnetic field conditions. *Journal of Geophysical Research: Space*  
499 *Physics*, *112*(A8). doi:10.1029/2007JA012270

500 Williams, D. J., Mauk, B., & McEntire, R. W. (1997). Trapped electrons in Ganymede's  
501 magnetic field. *Geophysical Research Letters*, *24*(23), 2953--2956.  
502 doi:10.1029/97GL03003

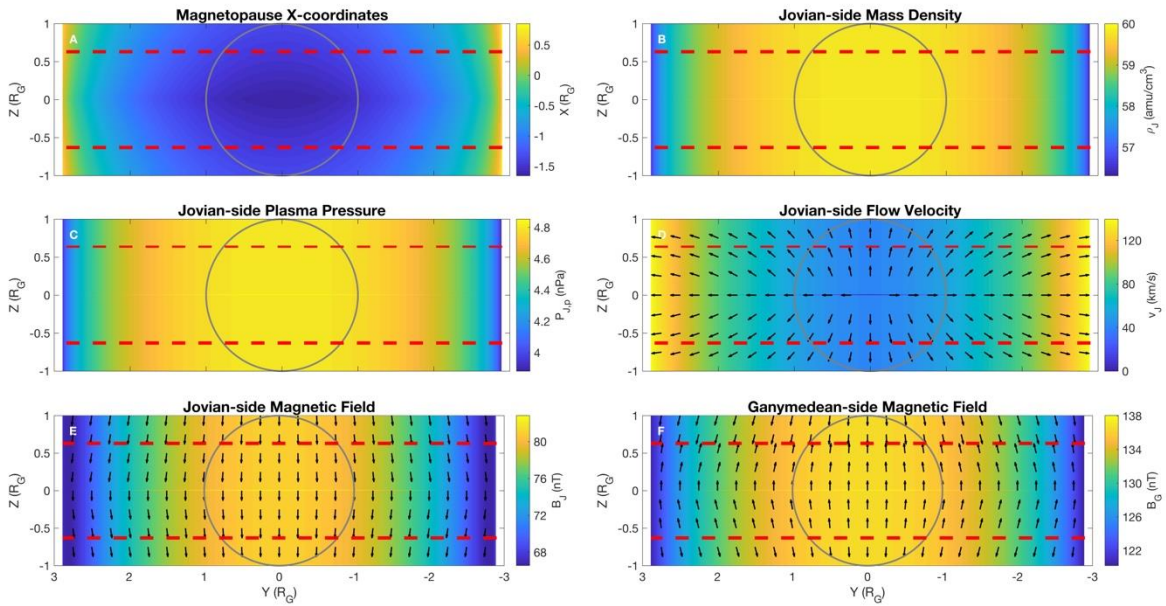
503 Williams, D. J., Mauk, B. H., McEntire, R. W., Roelof, E. C., Armstrong, T. P., Wilken, B., .  
504 . . . Murphy, N. (1997). Energetic particle signatures at Ganymede: Implications for  
505 Ganymede's magnetic field. *Geophysical Research Letters*, *24*(17), 2163--2166.  
506 doi:10.1029/97GL01931

507 Zarka, P., Soares Marques, M., Louis, C., Ryabov, V., Lamy, L., Echer, E., & Cecconi, B.  
508 (2018). Jupiter radio emission induced by Ganymede and consequences for the radio  
509 detection of exoplanets. *Astronomy & Astrophysics*. doi:10.1051/0004-  
510 6361/201833586

511 Zhou, H., Tóth, G., Jia, X., Chen, Y., & Markidis, S. (2019). Embedded Kinetic Simulation  
512 of Ganymede's Magnetosphere: Improvements and Inferences. *Journal of*  
513 *Geophysical Research: Space Physics*, *0*(0). doi:10.1029/2019JA026643



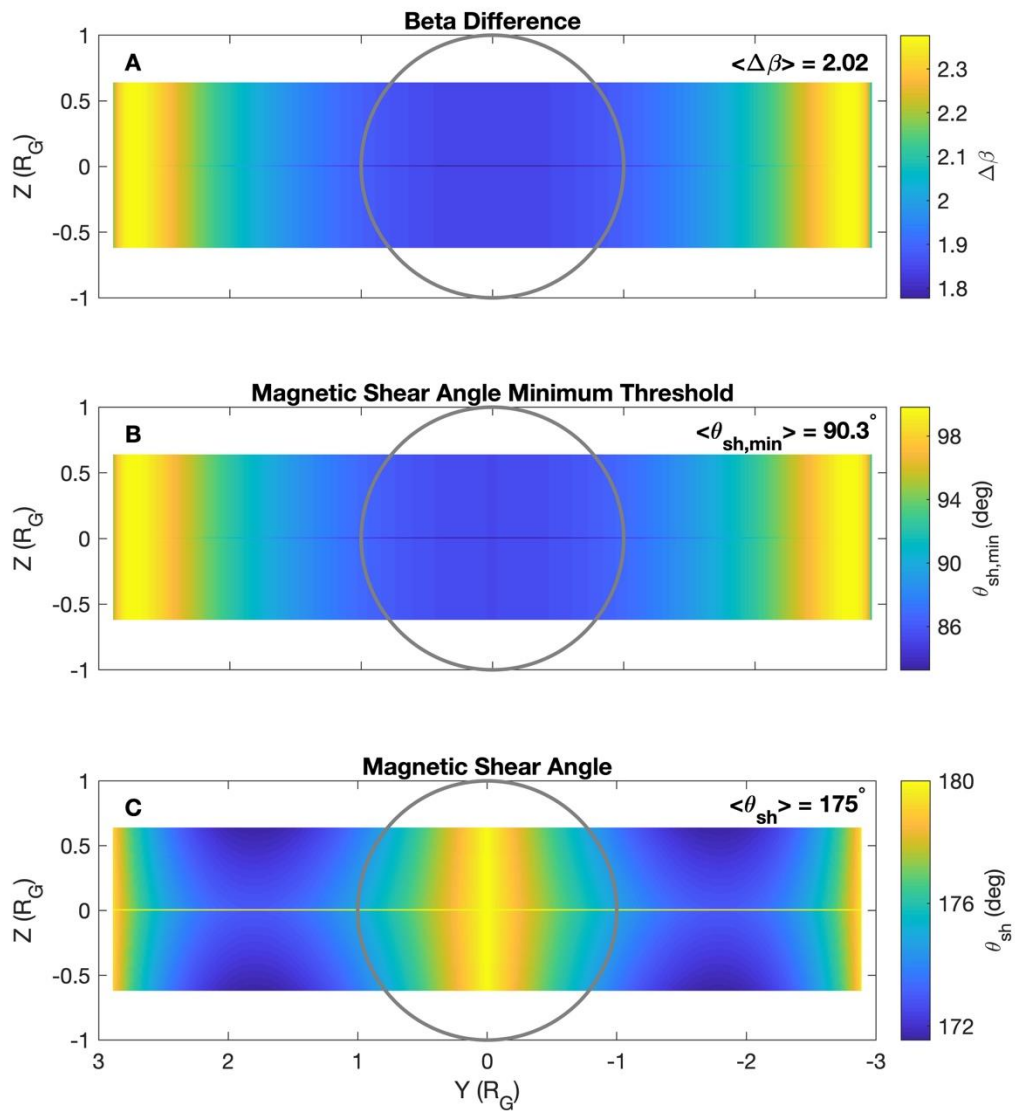
515



516

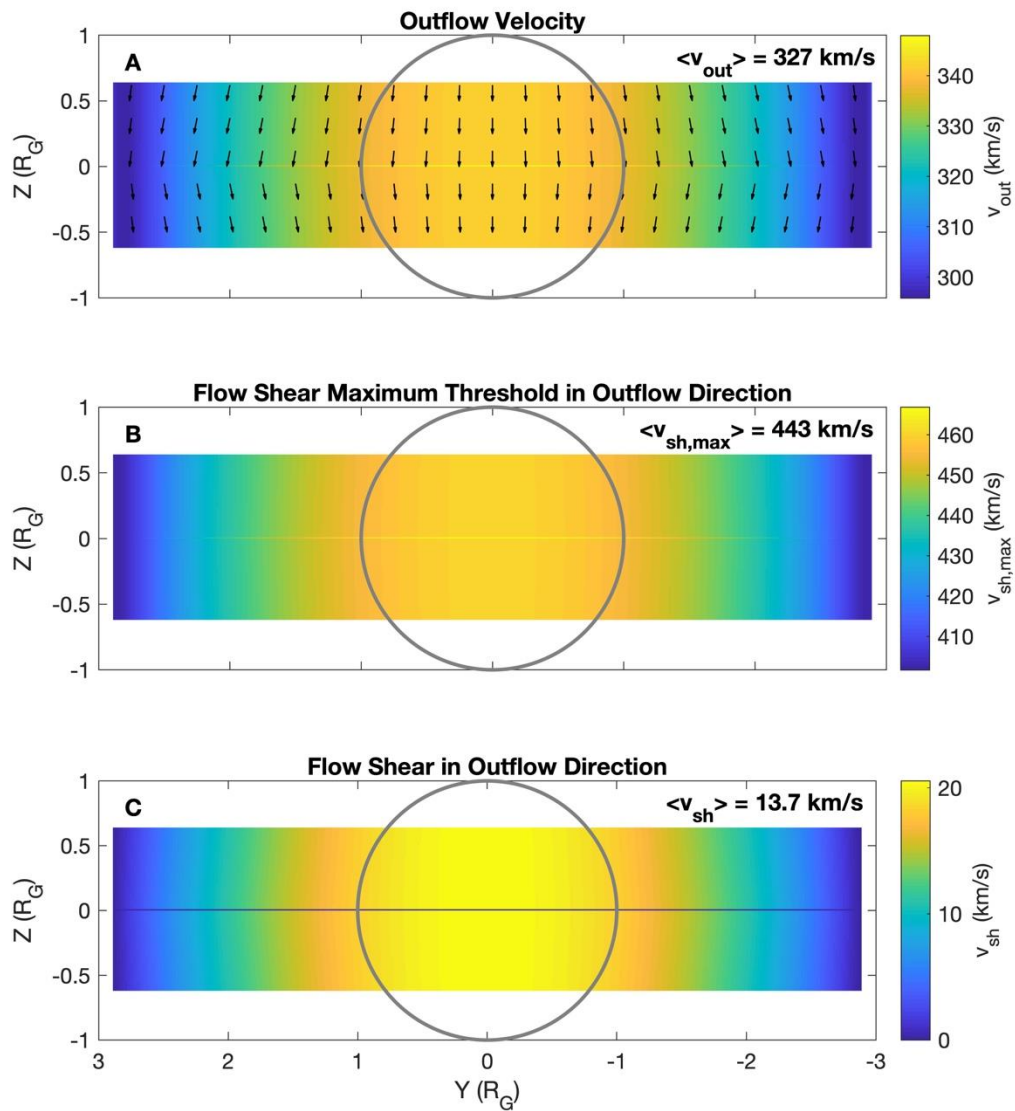
517 Figure 1: Magnetopause conditions projected onto a two-dimensional plane with the Jovian  
518 plasma flowing into the page when Ganymede is in the Jovian current sheet. Parameters  
519 shown are (A) X-coordinates on the magnetopause surface, (B) Jovian-side mass density, (C)  
520 Jovian-side plasma pressure, (D) Jovian-side flow velocity, (E) Jovian-side magnetic field,  
521 and (F) Ganymede-side magnetic field. Ganymede is outlined in grey and the closed-field  
522 region is defined between two red dashed lines.

523



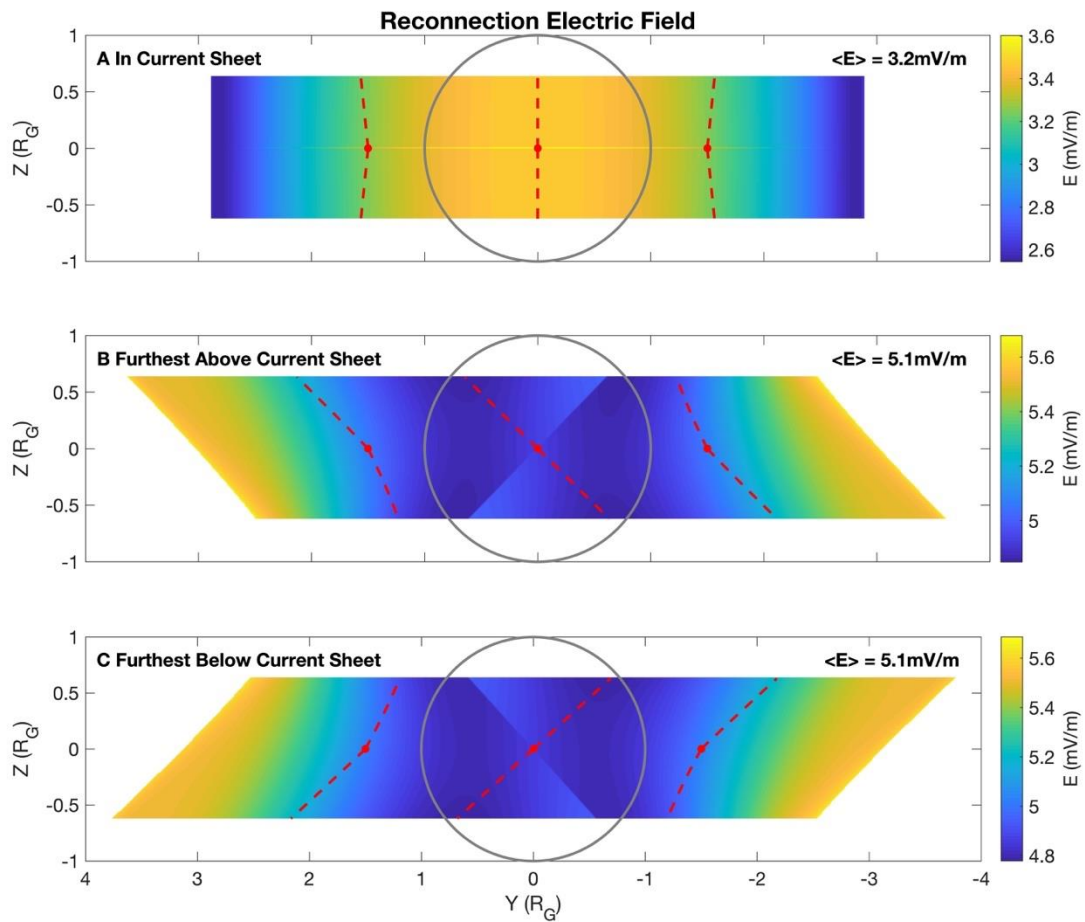
524

525 Figure 2: Evaluation of the diamagnetic drift onset condition in Ganymede's closed-field  
 526 region when Ganymede is in the Jovian current sheet. Parameters shown are (A) beta  
 527 difference across the magnetopause, (B) magnetic shear angle minimum threshold, and (C)  
 528 shear angle calculated from magnetopause conditions. Ganymede is outlined in grey and  
 529 average parameter values are shown at top right.



530

531 Figure 3: Evaluation of the bulk plasma flow shear onset condition in Ganymede's closed-  
 532 field regions when Ganymede is in the Jovian current sheet. Parameters shown are (A)  
 533 reconnection outflow velocity, (B) flow shear maximum threshold, and (C) flow shear  
 534 calculated from magnetopause conditions. The format is the same as Figure 2.



535

536 Figure 4: Electric field at potential reconnection sites in Ganymede's closed-field regions  
 537 computed when Ganymede is (A) in, (B) furthest above, and (C) furthest below the Jovian  
 538 current sheet. Red dashed lines indicate plasma outflow tracks from selected reconnection  
 539 sites. The format is the same as Figure 2.

540